Design and Observation of Biphase TiO2 Crystal with Perfect Junction

ARTICLE · SEPTEMBER 2014

1 AUTHOR:

Shengcai Zhu
Fudan University
2 PUBLICATIONS **3** CITATIONS

SEE PROFILE

THE JOURNAL OF PHYSICAL CHEMISTRY Letters

Letter

pubs.acs.org/JPCL

Design and Observation of Biphase TiO_2 Crystal with Perfect Junction

Sheng-Cai Zhu, Song-Hai Xie,* and Zhi-Pan Liu*

Shanghai Key Laboratory of Molecular Catalysis and Innovative Materials, Department of Chemistry, Key Laboratory of Computational Physical Science (Ministry of Education), Fudan University, Shanghai 200433, China

Supporting Information

ABSTRACT: Bicrystalline materials have wide applications from silicon chips to photocatalysis, but the controlled synthesis of nanocrytals with ordered phase junction has been challenging, in particular via chemical synesthetic routes. Here, we propose a general strategy to design biphase crystals formed via partial solid-to-solid phase transition with perfect phase junction, e.g., being atomically sharp and built of two particular sets of epitaxially joined planes of the two component phases, and present such an example by designing, synthesizing, and characterizing the interface of two TiO_2 phases, namely, TiO_2-B/anatase biphase nanocrystals that are obtained conveniently via one-pot chemical synthesis. Our design strategy classifies the common solid-to-solid phase transition into three types that are distinguishable by using the newly developed stochastic surface walking (SSW) method for unbiased pathway sampling. Only **Type-I** crystal is predicted to possess perfect phase junction, where the phase transition involves one and only one propagation direction featuring single pathway phase transition containing only one elementary kinetic step. The method is applicable for the understanding and the design of heterophase materials via partial phase transition in general.

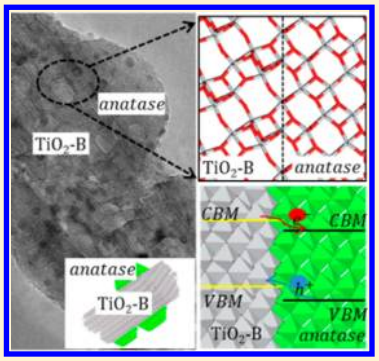

SECTION: Surfaces, Interfaces, Porous Materials, and Catalysis

The fabrication of bicrystalline materials has attracted much recent attention for their unique mechanical, optical,[1] and electrical properties.[2] In photocatalysis, for example, the presence of phase junction is also known to facilitate the separation of the photoexcited holes and electrons and boost the catalytic performance.[3] The structurally ordered phase boundary is important for this purpose since the defects can form charge traps and hinder the charge transfer. However, the synthesis of high quality biphase crystalline catalysts using (in)organic wet chemical methods has been challenging, in particular, how to control and optimize the structure of phase junction via partial phase transition is an open question. Here, we report a general strategy to design biphase crystals with ordered phase junction, e.g., lacking stacking faults or structural dislocations, based on the newly developed SSW pathway sampling method. This is exemplified by titania bicrystalline materials where the atomic nature of the phase junction is characterized by theoretical prediction via SSW pathway sampling and experimental observation using high-resolution transmission electron microscope (HRTEM).

The controlled synthesis of biphase nanocrystals with ordered interface is of great significance in photochemistry.[4,5] There are various synthetic methods to achieve heterophase junction structures, for example, via the straightforward partial solid-to-solid phase transition and the secondary seed-growth.[6−9] For the solid-to-solid phase transition, it requires the energetically favored phase separation and the stable phase boundary to glue crystals together. The presence of the structurally matched lattice or crystallographic planes is believed to be important to form the ordered phase junction. While the characterization of the phase junction is critical for identifying these crystallographic planes, if present, and for understanding the phase transition kinetics, the interface structure between phases is extremely difficult to resolve,[10] requiring atomic resolution at the junction experimentally and a detailed knowledge of the phase transition mechanism.

In this work, we propose a general scheme, as shown in Figure 1, to design biphase crystals via partial solid-to-solid phase transition that potentially have ordered phase junction based on newly developed stochastic surface walking (SSW) pathway sampling method.[11−13] The SSW pathway sampling for crystal can reveal the solid-to-solid transition pathways with explicitly located transitions states (TS) and thus provide important insights into the connectivity of the crystal phases on the potential energy surface (PES). Instead of traditional lattice matching criterion, our strategy is based on the low energy phase transition pathways obtainable from SSW pathway sampling simulation, where the energetics of the barrier height and the complexity of the pathway (i.e., one-step, multiple-step) are the key parameters for structure prediction.

Specifically, the low barrier (E_a) of the phase transformation is desirable for achieving a stable phase junction, which is a

Received: August 2, 2014
Accepted: September 2, 2014

   dx.doi.org/10.1021/jz5016247 | J. Phys. Chem. Lett. 2014, 5, 3162−3168

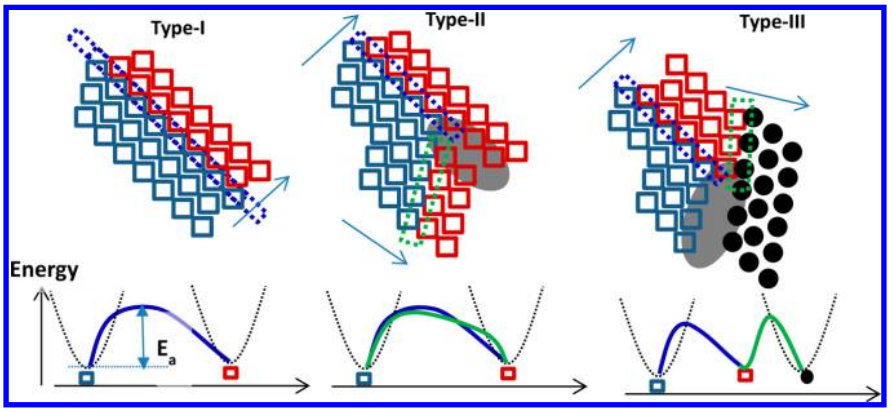

Figure 1. Strategy to design biphase crystals with ordered phase junction via the partial solid-to-solid phase transition based on SSW crystal phase transition pathways. **Type-I** crystal involves one and only one phase propagation direction often featured as a single-pathway one-step transition, which is predicted to possess ordered phase junction; **Type-II** crystal has multiple energetically degenerated reaction channels, and **Type-III** crystal has a multiple-step phase transition mechanism involving intermediate crystal phases, both of them having more than one phase propagation directions. The shaded areas in **Type-II** and **Type-III** crystals indicate where the stress develops during the phase junction propagation that eventually leads to large structural deformation of phase junction (e.g., cracking, stacking faults).

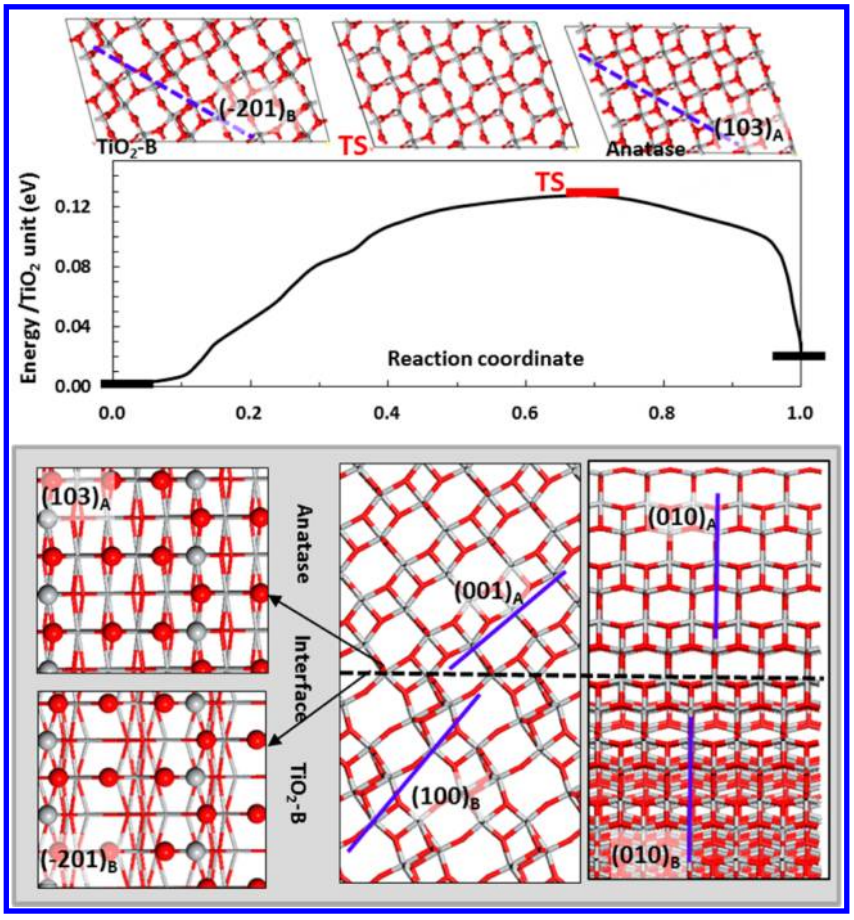

Figure 2. (Top panel) DFT lowest energy transition pathway from TiO_2-B to anatase bulk crystal (structures viewed down from the *b* axis). The blue lines indicate the habit plane of the phase transition. (Bottom panel) The atomic structure of the TiO_2-B/anatase phase junction with orientation relation $(\bar{2}01)_B//(103)_A + [010]_B//[010]_A$ as predicted from theory. From left to the right are the top-views of $(103)_A$ and $(\bar{2}01)_B$, and two side-views of the junction showing the $(100)_B$ together with $(001)_A$ (theoretical dihedral angle 11.0 degrees), and $(010)_B//(010)_A$. Ti: gray balls; O: red balls.

quantitative reflection of the lattice matching (low strain) of two phases. However, the nature of the pathway, i.e., the direction of the phase transition due to the anisotropy of crystal, could also be important. According to the complexity of the solid-to-solid transition pathways, we classify the common crystal-to-crytal phase transition into three basic types (see Figure 1) and propose a simple rule to design high quality biphase crystals, that is, to satisfy the **Type-I** phase transition condition, specifically, *the phase transition should propagate along one and only one direction (e.g., defined by a habit plane),*

dx.doi.org/10.1021/jz5016247 | *J. Phys. Chem. Lett.* 2014, 5, 3162−3168

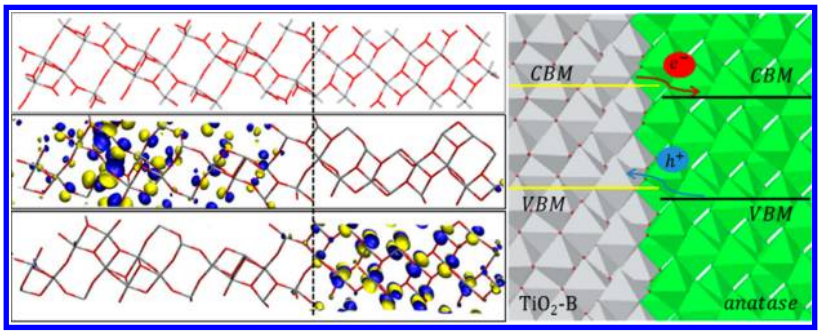

Figure 3. (Left) The structure and wave function of a superlattice biphase crystal, containing half−half TiO_2-B/anatase phases, showing the spatially well separated valence band maximum (middle) and the conduction band minimum (bottom). The dotted line indicates the interface. The isosurface density value of the plots is 0.02 e/bohr^3. (Right) The scheme for the band alignment between TiO_2-B (gray color) and anatase (green color) at the phase junction.

characterized as single pathway phase transition containing only one elementary kinetic step (the solid-to-solid phase transition occurs directly from one phase to another without any stable intermediate phases). In this way, the formed phase junction can be atomically sharp and built of two particular sets of epitaxially joined planes of the two component phases. The phase transitions along more than one propagation direction, due to the presence of either degenerate phase transition channels (the **Type-II** phase transition) or intermediate phases (the **Type-III** phase transition), are in principle not possible to yield biphase crystals with ordered phase junction due to the accumulated stress at the fronts of phase boundaries. As schematically illustrated in Figure 1, two junction fronts in **Type-II** and **Type-III** crystals cannot join smoothly at the junction−junction meeting areas (shaded in Figure 1) where the fracture or structural deformation (e.g., via stacking faults) is expected to develop to reduce the stress at the phase boundaries.[14,15]

It should be mentioned that the heterostructured nanocrystals with multiple phases can be synthesized by alternative technics other than the direct partial phase-transition, e.g., most commonly by heterogeneous nucleation of a secondary phase on top of a preformed primary phase.[4,6,9] These seeded-growth approaches could also produce high quality heterointerfaces, even highly strained, for the kinetic reasons.[8,9] The synthetic conditions are thus critical to the kinetics, such as the growth rate and the initial exposing facets.[16] Obviously, our design strategy does not apply to this category of phase junctions.

To demonstrate this design strategy and look for the **Type-I** crystal-to-crystal phase transition, we have explored the likely phase transition pathways of TiO_2 crystal using SSW,[11−13] including all common TiO_2 phases, e.g., rutile, anatase, brookite, and TiO_2-B, without assuming any reaction coordinates or imposing symmetry constraints. TiO_2 is selected as the example for the biphase crystal design because TiO_2 has a range of different phases, and the biphase TiO_2 crystals have a wide application as photocatalysts.[17] Among a large data set of phase transition pathways searched for TiO_2 phases, we identify the TiO_2-B-to-antase phase transition fulfilling the **Type-I** criterion. While the atomic structure of the phase junction for TiO_2-B/anatase crystal is not yet determined, the main focus of the work is thus to characterize the phase junction using SSW simulation and experiment to verify the theory on the biphase crystal design. By synthesizing the TiO_2-B/anatase biphase crystals using different chemical synthetic methods, we will show that the TiO_2-B/anatase phase junction is prevalently perfect, i.e., free of stacking faults or defects, where the theoretical model and experimental observation by HRTEM is highly consistent.

Taking the TiO_2-B phase as the example, the crystal extension of the SSW method (SSW-crystal) developed recently[11−13] is first utilized to sample the likely phase transition pathways leaving TiO_2-B. All calculation details are described in the Supporting Information (SI) and briefly outlined below. The pathway sampling was carried out initially using the classical Matsui−Akaogi interatomic potential[18] starting from the TiO_2-B phase (8 TiO_2 units per cell) to generate a database of pathways that connect TiO_2-B with the other phases. In total, 4500 pathways were collected from 5000 SSW-crystal steps of pathway sampling. While the majority of the pathways (500) were found to convert TiO_2-B to anatase, the other pathways leading to the phases such as rutile were also identified. The first-principles density functional theory (DFT) calculations based on the variable-cell double-ended surface walking method[19] were then utilized to verify the energetics of every low energy pathways, from which the lowest energy reaction pathway is obtained.

The lowest energy pathway leaving the TiO_2-B phase is the connection between TiO_2-B and anatase, which is a one-step transition, and the other transition pathways leaving TiO_2-B phase are energetically much higher. The reaction profile is shown in Figure 2, highlighting the late TS and the smooth lattice-distortive transformation, starting from a TiO_2-B lattice (a = 12.207, b = 3.769, c = 6.645 Å, $\alpha = \gamma = 90°$, β = 75.644°) to an anatase lattice (a = 10.522, b = 3.812, c = 7.625 Å, $\alpha = \gamma = 90°$, β = 68.865°). We noticed that the TiO_2-B-to-anatase pathway is much simpler compared to the anatase-to-rutile phase transition pathway, a three-step phase transition with two high pressure phases, MI and TiO_2II, as the intermediates. The calculated barrier is low, only 0.12 eV per TiO_2 unit from DFT, about half of that in the anatase-to-rutile phase transition,[13] indicating that the TiO_2-B to anatase transition is more facile compared to the anatase-to-rutile phase transition. This was indeed observed in experiment, where the phase transition starts above 673 K from TiO_2-B to anatase but it is more than 873 K for anatase-to-rutile.[20]

By closely inspecting the TiO_2-B to anatase crystal transition pathway, we can identify the habit planes of the phase transition (blue dotted line, Figure 2), being the crystal planes $TiO_2B(\bar{2}01)$ and anatase(103), which supports that the phase transition basically follows the diffusionless Martensitic mechanism together with short-ranged displacement of Ti and O ions. The orientation relationship of TiO_2-B/anatase phases is thus determined to be $(\bar{2}01)_B//(103)_A$ + $[010]_B//$

dx.doi.org/10.1021/jz5016247 | J. Phys. Chem. Lett. 2014, 5, 3162−3168

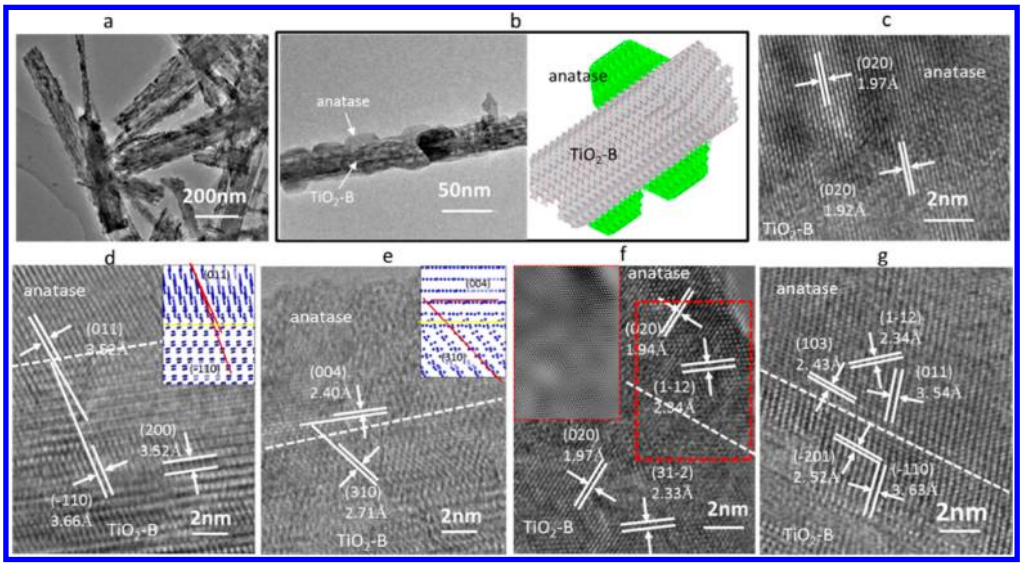

Figure 4. TEM (a–b) and HRTEM (c–g) images of the phase junction between anatase and TiO_2-B. In the HRTEM images, c–e belong to one crystal, and f–g belong to another. (b) The TiO_2-B/anatase nanofiber and the atomic model. (c) $(020)_A//(020)_B$; (d) $(011)_A$ and $(\bar{1}10)_B$ (angle 6°); (e) $(004)_A$ and $(310)_B$ (angle 48°). The theoretical structure of the junction (only showing Ti ions as blue dots) are shown in the top-right corner in panels d–e to compare with the experiment. (f) $(1\bar{1}2)_A//(31\bar{2})_B$ and $(020)_A//(020)_B$. The insert in (f) is the inverse fast Fourier transform (IFFT) of the junction area indicated by the red box, showing the perfect structure transition from one phase to another. (g): The habit planes, $(103)_A//(\bar{2}01)_B$ together with $(\bar{1}10)_B$, $(011)_A$, and $(\bar{1}12)_A$ planes.

$[010]_A$. From the orientation relationship, we can construct a theoretical model for the phase junction, as shown in Figure 2. Although the habit planes, $(\bar{2}01)_B//(103)_A$, are highly corrugated, the phase junction exhibits a closely matched lattice and similar atomic registration between the two phases.

Based on the theoretical model, a superlattice biphase crystal comprising both TiO_2-B and anatase is thus constructed and optimized using DFT, which enables us to provide insight into the electronic structure of the biphase crystal. Shown in Figure 3 is such a biphase crystal composing half TiO_2–B and half anatase (one unit cell). Our calculation shows that the strain introduced by the interface is very low, below 2%, and the shortest Ti–O distance at the junction is also less than 2.3% different from the bulk phases.

Importantly, the TiO_2–B/anatase bicrystal possesses spatially separated valence band maximum (VMB) and conduction band minimum (CBM), as shown in Figure 3, left. The VBM where the photogenerated hole resides is dominantly accumulated on the TiO_2-B side, while the CBM where the photogenerated electron stays is mainly populated on the anatase side. Obviously, the presence of the ordered phase junction leads to the shrinking of band gap in the biphase crystal and a new anisotropic behavior of electron/hole transfer, that is, the hole transfers to TiO_2-B while the electron goes oppositely toward anatase along the habit plane direction (Figure 3, right). This is an important optical property, which can significantly reduce the possibility for the electron–hole pair recombination and thus increase the quantum efficiency of the material.

It should be mentioned that the TiO_2-B/anatase system has been studied previously by many research groups. and most of them obtained the phase junction via the partial phase transition.[21−27] To date, the phase junction structure at the atomic level remains unknown, and the orientation relation is highly controversial (see SI Table S1). Two representative orientation relations suggested recently based on HRTEM observations are $[010]_A//[010]_B + [001]_A//[100]_B$ reported by Li et al.[23] ([*uvw*] represents the real space vector), and $[010]_A// [010]_B + (001)_A//(100)_B$ suggested by Yang et al. We found that the atomic model for the interface constructed according to these assignments cannot maintain the octahedron unit of Ti ions with either too close contact between Ti ions or O ions (see Figure S1 in the SI), and thus the proposed interface atomic structures are unlikely. In fact, a very early study by Brohan[28] identified $a(\bar{2}01)_B//(10\bar{3})_A$ orientation relation based only on the electron diffraction pattern, and our current theoretical results are consistent with the diffraction pattern.

Having the atomic structure of phase junction from theory, we then verify the structure by experiment. Our experimental procedure to synthesize TiO_2-B nanowire using $H_2Ti_3O_7$ as the precursor is as those described previously.[29,30] The $H_2Ti_3O_7$ fibers can transform partially to anatase nanocrystals at the hydrothermal condition (the wet condition), and the TiO_2-B/anatase bicrystalline can then be obtained after a low temperature (673 K) calcination.[31,32] Alternatively, the TiO_2-B/anatase can form directly via the solid–solid phase transition by heating the dry TiO_2-B fibers to 873 K (dry conditions),[33] which is obtained from the hydrothermal synthesis. We have synthesized the TiO_2–B/anatase bicrystalline samples via both methods. The identity of the phases (TiO_2-B and anatase crystalline) is verified by XRD patterns, and the structure is further characterized using TEM and HRTEM. The experimental synthetic procedure and the supporting data are detailed in the SI. Typical examples of the bicrystalline material are shown in Figure 4a,b, where the anatase nanocrystals attach on the top of the TiO_2-B nanowires. We found that both synthetic methods produce the same phase junction structure, being consistent at the atomic level, as revealed by HRTEM. Below we present the results for the phase junction from the samples synthesized under wet conditions (those from dry conditions are shown in the SI).

Figure 4 illustrates five different zone-axis patterns (c–g) of HRTEM originated from two different crystals (c–e belong to one crystal, and f–g belong to another), and the important data

dx.doi.org/10.1021/jz5016247 | J. Phys. Chem. Lett. 2014, 5, 3162–3168

on the interplanar *d*-spacing and dihedral angles are indicated. The atomic model from theory is compared with every HRTEM image (see Figure 4 and also the SI), and the results on dihedral angles are detailed in Table 1. Figure 4c shows that

Table 1. Dihedral Angles between the Crystallographic Planes of Two Phases Measured by Experiment (HRTEM in Figure 4) and Predicted by Theory

TiO_2-B	anatase	experiment (±1°)	theory (deg)
(020)	(020)	0	0.0
$(\bar{2}01)$	(103)	0	0.0
$(\bar{1}10)$	(011)	6	5.3
(310)	(004)	48	47.0
(100)	(020)	90	90.0
(020)	(004)	90	90.0
$(31\bar{2})$	$(1\bar{1}2)$	179	179.3

the $(010)_B$ plane is parallel with the $(010)_A$ plane, which is as expected from the theoretical orientation relationship. Because the *d*-spacing of the two surface planes are almost identical (difference <0.05 Å), it is essentially impossible to distinguish the interface.

By rotating the zone axis, we are able to observe a set of other surface planes, which can reveal the atomic detail of the phase junction. In Figure 4d,e, the phase junction exhibits the other surface planes, where the dihedral angle of the planes can be measured directly from the images, i.e., the dihedral angles between $(011)_A$ and $(\bar{1}10)_B$, and between $(004)_A$ and $(310)_B$. The theoretical values for these angles are 5.3° and 47.0°, which are essentially identical to those measured from the HRTEM image (6° and 48°). Figure 4f,g shows the three sets of planes that are parallel with each other, namely, $(1\bar{1}2)_A//(31\bar{2})_B$ (approximately parallel, Table 1), $(020)_A//(020)_B$, and $(103)_A//(\bar{2}01)_B$ (the habit planes), as also predicted from theory. The inset in panel f highlights the junction area with inverse fast Fourier transform (IFFT), which show a perfect structure transition from one phase to another. Based on the agreement between theory and experiment on a large data set of experimental images (Table 1 and also see the SI), we conclude that the TiO_2-B/anatase phase junction can be regarded as a perfect phase junction that lacks the common stacking faults or dislocation defects otherwise commonly present during the growth and packing of crystals.[34]

To provide insight into the kinetics of the phase transition and the origin of the perfect phase junction, we performed SSW global optimization and the pathway sampling simulations starting from different TiO_2-B surfaces. Owing to the constraint by the lattice of the underlying TiO_2-B phase, the surface phase transition sampling mimics the constrained Martensitic phase transition of a solid at elevated temperatures (under dry conditions). Among a set of surface facets of TiO_2-B explored by SSW global optimization, including $(100)_B$, $(001)_B$, and $(\bar{2}01)_B$, only the $(\bar{2}01)_B$ exhibits the phase transition toward the anatase phase, resulting in the formation of $(103)_A$. The results are consistent with the habit planes identified from the bulk simulation. The initial phase transition pathways were then searched using SSW pathway sampling, and it turns out that one and only one low energy channel (with the barrier lower than 1 eV) is identified from more than 10^3 transition pathways collected. The other reaction channels to reconstruct the surface, e.g., forming structural defects, are energetically much disfavored.

The DFT energy profile for the lowest energy pathway is shown in Figure 5 together with the snapshots of the located

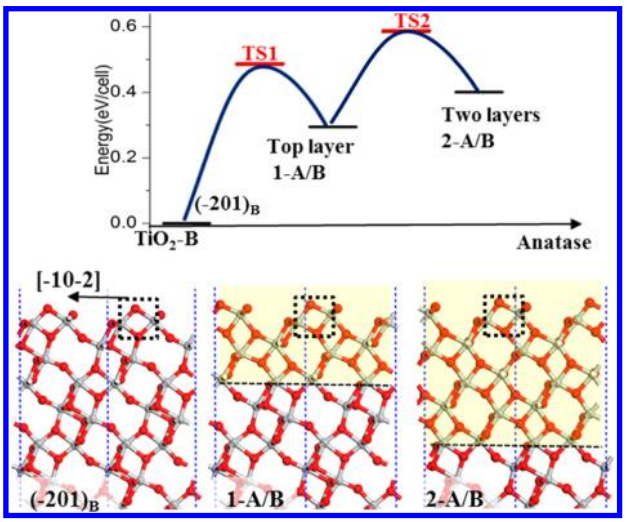

Figure 5. DFT energy profile and the structure snapshots for the lowest energy pathway from TiO_2-B to a two-layer anatase-capped TiO_2-B initiating from the $(\bar{2}01)_B$ surface. The dotted lines indicate the interface, and the colored areas in 1-A/B and 2-A/B are the newly formed anatase phase. The dotted boxes highlight the characteristic TiO unit moving along $[\bar{1}0\bar{2}]_B$ in phase transition.

intermediates. The simulation shows that the phase transition initiates from the TiO_2-B $(\bar{2}01)_B$ surface and propagates layer-by-layer from the surface to the bulk, involving the atoms gliding smoothly along the $[\bar{1}0\bar{2}]_B$ direction (arrow in Figure 5). The calculated barrier for forming the first layer anatase is 0.49 eV per $p(1 \times 1)$ cell from DFT and the overall barrier to form two layers of anatase is slightly higher, being 0.58 eV. This indicates that the propagation of the anatase phase into TiO_2-B bulk is not instantaneous but kinetically self-limiting, requiring elevated temperature to allow the junction front ripple into bulk TiO_2-B layer-by-layer, as observed in our experiment. The single pathway for the phase transition revealed from pathway sampling can thus be correlated with the observation of the perfect phase junction between TiO_2-B and anatase, which could then rationalize the enhancement of photoactivity of the biphase TiO_2-B/anatase material, as reported previously[25] and also confirmed in our experiment (see SI Figure S12). Our results indicate that the chemical synthesis of heterophase crystals with perfect junction is feasible as long as the phase transition is kinetically controlled by a one-step layer-by-layer propagation mechanism.

In nature, there are other types of phase transitions as classified in Figure 1. The anatase-to-rutile phase transition of TiO_2, for example, belongs to the Type-III phase transition, where two intermediate phases, MI and TiO_2II, are present in the lowest energy pathway. Two sets of habit planes, i.e. anatase-to-TiO_2II (anatase(112)//TiO_2II(100)) and TiO_2II-to-rutile (rutile(011)//TiO_2II(001)) are involved in phase transition and not parallel with each other but rotated by 90° (detailed in our recent work[13] and the SI), and thus two different phase junctions, anatase/TiO_2II and TiO_2II/rutile, propagate orthogonally. Our experiment based on HRTEM observation of anatase/rutile biphase samples prepared in one-pot synthesis indeed shows that the phase junction of anatase/rutile can not be perfect. The theoretical dihedral angles deviate

dx.doi.org/10.1021/jz5016247 | J. Phys. Chem. Lett. 2014, 5, 3162−3168

from the measured values for a set of crystallographic planes from HRTEM by up to 13° (see SI Figure S13 for details), being much larger than that of TiO_2-B/anatase samples. The nature of the imperfect interface structure is the focus of our onging work.

The design strategy for biphase crystal presented here establishes a fundamental connection between the "invisible" PES of crystal and the "visible" atomic structure of the phase junction. A simple connectivity between phases, i.e., low barrier, single pathway, and one-step transition, is the key for the one-pot chemical synthesis of biphase crystals with ordered phase junction via partial phase transition. The unbiased PES sampling using SSW methods can facilitate the understanding of the solid-to-solid phase transition and the design of new materials in general.

■ ASSOCIATED CONTENT

Supporting Information

The SSW-crystal pathway sampling method and the calculation detail; the experimental procedure to synthesize biphase crystals and the experimental data (XRD, HRTEM) for characterizing the biphase crystals prepared at the dry conditions; the HRTEM results on the phase junction of rutile/anatase; and the photoactivity test of TiO_2−B/anatase biphase sample. This material is available free of charge via the Internet at http://pubs.acs.org.

■ AUTHOR INFORMATION

Corresponding Authors

*E-mail: shxie@fudan.edu.cn (S.H.X.).
*E-mail: zpliu@fudan.edu.cn (Z.P.L.).

Notes

The authors declare no competing financial interest.

■ ACKNOWLEDGMENTS

This work is supported by the National Science Foundation of China (21173051, 21361130019), 973 program (2011CB808500, 2013CB834603), the Science and Technology Commission of Shanghai Municipality (08DZ2270500), and the Program for Professor of Special Appointment (Eastern Scholar) at Shanghai Institute of Higher Learning.

■ REFERENCES

(1) Kawahara, T.; Konishi, Y.; Tada, H.; Tohge, N.; Nishii, J.; Ito, S. A Patterned TiO_2 (Anatase)/TiO_2 (Rutile) Bilayer-Type Photocatalyst: Effect of the Anatase/Rutile Junction on the Photocatalytic Activity. *Angew. Chem.* **2002**, *114*, 2935−2937.

(2) Chiang, Y. M.; Silverman, L. A.; French, R. H.; Cannon, R. M. Thin Glass Film between Ultrafine Conductor Particles in Thick-Film Resistors. *J. Am. Ceram. Soc.* **1994**, *77*, 1143−1152.

(3) Zhang, J.; Xu, Q.; Feng, Z.; Li, M.; Li, C. Importance of the Relationship between Surface Phases and Photocatalytic Activity of TiO_2. *Angew. Chem., Int. Ed.* **2008**, *47*, 1766−1769.

(4) Hurum, D.; Agrios, A.; Crist, S.; Gray, K.; Rajh, T.; Thurnauer, M. Probing Reaction Mechanisms in Mixed Phase TiO_2 by EPR. *J. Electron Spectrosc. Relat. Phenom.* **2006**, *150*, 155−163.

(5) Yang, D. J.; Liu, H. W.; Zheng, Z. F.; Yuan, Y.; Zhao, J. C.; Waclawik, E. R.; Ke, X. B.; Zhu, H. Y. An Efficient Photocatalyst Structure: TiO_2(B) Nanofibers with a Shell of Anatase Nanocrystals. *J. Am. Chem. Soc.* **2009**, *131*, 17885−17893.

(6) Carbone, L.; Cozzoli, P. D. Colloidal Heterostructured Nanocrystals: Synthesis and Growth Mechanisms. *Nano Today* **2010**, *5*, 449−493.

(7) Casavola, M.; Buonsanti, R.; Caputo, G.; Cozzoli, P. D. Colloidal Strategies for Preparing Oxide-Based Hybrid Nanocrystals. *Eur. J. Inorg. Chem.* **2008**, 837−854.

(8) Buonsanti, R.; Grillo, V.; Carlino, E.; Giannini, C.; Gozzo, F.; Garcia-Hernandez, M.; Garcia, M. A.; Cingolani, R.; Cozzoli, P. D. Architectural Control of Seeded-Grown Magnetic-Semicondutor Iron Oxide−TiO_2 Nanorod Heterostructures: The Role of Seeds in Topology Selection. *J. Am. Chem. Soc.* **2010**, *132*, 2437−2464.

(9) Buonsanti, R.; Grillo, V.; Carlino, E.; Giannini, C.; Curri, M. L.; Innocenti, C.; Sangregorio, C.; Achterhold, K.; Parak, F. G.; Agostiano, A.; et al. Seeded Growth of Asymmetric Binary Nanocrystals Made of a Semiconductor TiO_2 Rodlike Section and a Magnetic Gamma-Fe_2O_3 Spherical Domain. *J. Am. Chem. Soc.* **2006**, *128*, 16953−16970.

(10) Chua, A. L.-S.; Benedek, N. A.; Chen, L.; Finnis, M. W.; Sutton, A. P. A Genetic Algorithm for Predicting the Structures of Interfaces in Multicomponent Systems. *Nat. Mater.* **2010**, *9*, 418−422.

(11) Shang, C.; Liu, Z.-P. Stochastic Surface Walking Method for Structure Prediction and Pathway Searching. *J. Chem. Theory Comput.* **2013**, *9*, 1838−1845.

(12) Zhang, X.-J.; Shang, C.; Liu, Z.-P. From Atoms to Fullerene: Stochastic Surface Walking Solution for Automated Structure Prediction of Complex Material. *J. Chem. Theory Comput.* **2013**, *9*, 3252−3260.

(13) Shang, C.; Zhang, X.-J.; Liu, Z.-P. Stochastic Surface Walking Method for Crystal Structure and Phase Transition Pathway Prediction. *Phys. Chem. Chem. Phys.* **2014**, *16*, 17845.

(14) Capolungo, L.; Spearot, D.; Cherkaoui, M.; McDowell, D.; Qu, J.; Jacob, K. Dislocation Nucleation from Bicrystal Interfaces and Grain boundary Ledges: Relationship to Nanocrystalline Deformation. *J. Mech. Phys. Solids* **2007**, *55*, 2300−2327.

(15) Gilbert, B.; Huang, F.; Zhang, H.; Waychunas, G. A.; Banfield, J. F. Nanoparticles: Strained and Stiff. *Science* **2004**, *305*, 651−654.

(16) Shim, M.; McDaniel, H. Anisotropic Nanocrystal Heterostructures: Synthesis and Lattice Strain. *Curr. Opin. Solid State Mater. Sci.* **2010**, *14*, 83−94.

(17) Grätzel, M. Photoelectrochemical Cells. *Nature* **2001**, *414*, 338−344.

(18) Matsui, M.; Akaogi, M. Molecular Dynamics Simulation of the Structural and Physical Properties of the Four Polymorphs of TiO_2. *Mol. Simul.* **1991**, *6*, 239−244.

(19) Zhang, X. J.; Shang, C.; Liu, Z. P. Double-Ended Surface Walking Method for Pathway Building and Transition State Location of Complex Reactions. *J. Chem. Theory Comput.* **2013**, *9*, 5745−5753.

(20) Zhang, H.; Banfield, J. F. New Kinetic Model for the Nanocrystalline Anatase-to-Rutile Transformation Revealing Rate Dependence on Number of Particles. *Am. Mineral.* **1999**, *84*, 528−535.

(21) Liu, B.; Khare, A.; Aydil, E. S. TiO_2-B/Anatase Core-Shell Heterojunction Nanowires for Photocatalysis. *ACS Appl. Mater. Interfaces* **2011**, *3*, 4444−4450.

(22) Yoshida, R.; Suzuki, Y.; Yoshikawa, S. Syntheses of TiO_2(B) Nanowires and TiO_2 Anatase Nanowires by Hydrothermal and Post-heat Treatments. *J. Solid State Chem.* **2005**, *178*, 2179−2185.

(23) Li, W.; Liu, C.; Zhou, Y.; Bai, Y.; Feng, X.; Yang, Z.; Lu, L.; Lu, X.; Chan, K.-Y. Enhanced Photocatalytic Activity in Anatase/TiO_2(B) Core−Shell Nanofiber. *J. Phys. Chem. C* **2008**, *112*, 20539−20545.

(24) Bai, Y.; Li, W.; Liu, C.; Yang, Z. H.; Feng, X.; Lu, X. H.; Chan, K. Y. Stability of Pt Nanoparticles and Enhanced Photocatalytic Performance in Mesoporous Pt-(Anatase/TiO_2(B) Nanoarchitecture. *J. Mater. Chem.* **2009**, *19*, 7055−7061.

(25) Zhou, W. J.; Gai, L. G.; Hu, P. G.; Cui, J. J.; Liu, X. Y.; Wang, D. Z.; Li, G. H.; Jiang, H. D.; Liu, D.; Liu, H.; et al. Phase Transformation of TiO_2 Nanobelts and TiO_2(B)/Anatase Interface Heterostructure Nanobelts with Enhanced Photocatalytic Activity. *CrystEngComm* **2011**, *13*, 6643−6649.

(26) Zheng, Z. F.; Liu, H. W.; Ye, J. P.; Zhao, J. C.; Waclawik, E. R.; Zhu, H. Y. Structure and Contribution to Photocatalytic Activity of the Interfaces in Nanofibers with Mixed Anatase and TiO_2(B) Phases. *J. Mol. Catal. A: Chem.* **2010**, *316*, 75−82.

(27) Huang, C. X.; Zhu, K. R.; Qi, M. Y.; Zhuang, Y. L.; Cheng, C. Preparation and Photocatalytic Activity of Bicrystal Phase TiO_2 Nanotubes Containing TiO_2-B and Anatase. *J. Phys. Chem. Solids* **2012**, *73*, 757−761.
(28) Brohan, L.; Verbaere, A.; Tournoux, M.; Demazeau, G. La Transformation TiO_2(B)→ Anatase. *Mater. Res. Bull.* **1982**, *17*, 355−361.
(29) Armstrong, A. R.; Armstrong, G.; Canales, J.; Bruce, P. G. TiO_2-B Nanowires. *Angew. Chem., Int. Ed. Engl.* **2004**, *43*, 2286−8.
(30) Armstrong, A. R.; Armstrong, G.; Canales, J.; García, R.; Bruce, P. G. Lithium-Ion Intercalation into TiO_2-B Nanowires. *Adv. Mater.* **2005**, *17*, 862−865.
(31) Zhu, H.; Gao, X.; Lan, Y.; Song, D.; Xi, Y.; Zhao, J. Hydrogen Titanate Nanofibers Covered with Anatase Nanocrystals: A Delicate Structure Achieved by the Wet Chemistry Reaction of the Titanate Nanofibers. *J. Am. Chem. Soc.* **2004**, *126*, 8380−8381.
(32) Tsai, C. C.; Teng, H. S. Structural Features of Nanotubes Synthesized from NaOH Treatment on TiO_2 with Different Post-treatments. *Chem. Mater.* **2006**, *18*, 367−373.
(33) Kuo, H.-L.; Kuo, C.-Y.; Liu, C.-H.; Chao, J.-H.; Lin, C.-H. A Highly Active Bi-crystalline Photocatalyst Consisting of TiO_2(B) Nanotube and Anatase Particle for Producing H_2 Gas from Neat Ethanol. *Catal. Lett.* **2007**, *113*, 7−12.
(34) Penn, R. L. Imperfect Oriented Attachment: Dislocation Generation in Defect-Free Nanocrystals. *Science* **1998**, *281*, 969−971.